Geophysical Research Letters

RESEARCH LETTER
10.1029/2020GL087528

Key Points:
- A new method of constructing a tropical cyclone intensity adjustment factor for global climate model simulations is proposed
- The new intensity adjustment factor uses high-resolution tropical cyclone simulations and is horizontal resolution-dependent
- Using the new adjustment indicates the low-intensity bias in global climate model-simulated tropical cyclones might be slightly exaggerated

A New Method to Construct a Horizontal Resolution-Dependent Wind Speed Adjustment Factor for Tropical Cyclones in Global Climate Model Simulations

Yumin Moon[1], Daehyun Kim[1], Suzana J. Camargo[2], Allison A. Wing[3], Kevin A. Reed[4], Michael F. Wehner[5], and Ming Zhao[6]

[1]Department of Atmospheric Sciences, University of Washington, Seattle, WA, USA, [2]Lamont-Doherty Earth Observatory, Columbia University, Palisades, NY, USA, [3]Department of Earth, Ocean, and Atmospheric Science, Florida State University, Tallahassee, FL, USA, [4]School of Marine and Atmospheric Sciences, Stony Brook University, Stony Brook, NY, USA, [5]Lawrence Berkeley National Laboratory, Berkeley, CA, USA, [6]NOAA Geophysical Fluid Dynamics Laboratory, Princeton, NJ, USA

Correspondence to:
D. Kim,
daehyun@uw.edu

Citation:
Moon, Y., Kim, D., Camargo, S. J., Wing, A. A., Reed, K. A., Wehner, M. F., & Zhao, M. (2020). A new method to construct a horizontal resolution-dependent wind speed adjustment factor for tropical cyclones in global climate model simulations. *Geophysical Research Letters*, *46*, e2020GL087528. https://doi.org/10.1029/2020GL087528

Received 18 FEB 2020
Accepted 15 MAY 2020
Accepted article online 19 MAY 2020

Abstract A new method to construct a horizontal resolution-dependent wind speed adjustment factor for evaluating tropical cyclones (TCs) in global climate models (GCMs) is presented. In contrast to the previous studies that used idealized axisymmetric wind fields, this study analyzes 48 hr of 10-s surface wind fields from 1-km TC simulations. The adjustment factor is derived from filtering the simulated TC wind fields onto various horizontal grid spacings typical of those used in GCMs. The new adjustment factor leads to TCs with greater intensity than the existing adjustment factors for horizontal grid spacings smaller than 30 km. This difference is attributed to more realistic wind fields in the TC simulations that contain highly asymmetric, localized patches of higher wind speeds instead of axisymmetric wind fields. Applying the new adjustment factor to select GCM simulations suggests the common interpretation of low-intensity bias in GCM-simulated TCs might be slightly exaggerated.

Plain Language Summary It has long been recognized that the intensity of tropical cyclones (maximum sustained surface wind speed) in global climate model simulations needs adjustments as the horizontal grid spacing of the climate models is not yet fine enough, resulting in the representative errors in the simulated tropical cyclone structures. This study presents a new method to construct a horizontal resolution-dependent tropical cyclone intensity adjustment factor that can be used when evaluating tropical cyclones in climate model simulations. Our new method uses tropical cyclone simulations performed with 1-km horizontal grid spacing, in which tropical cyclone structures are realistically captured. Applying the new adjustment factor increases the interpreted intensity of simulated tropical cyclones, which suggests that the common interpretation of low-intensity bias in climate model-simulated tropical cyclones in comparison to the observations might be slightly exaggerated.

1. Introduction

How tropical cyclone (TC) activity—such as frequency, intensity distribution, and tracks—will change in a warming climate has been the subject of numerous studies in the past (e.g., Bindoff et al., 2013; Knutson et al., 2010; Knutson et al., 2019; Walsh et al., 2016). Global climate models (GCMs) have been an indispensable tool in this endeavor, especially after continued improvements in computational power and numerical methods have made it more attainable to perform long-term GCM simulations of TCs with horizontal grid spacing of half degree or less (e.g., Camargo & Wing, 2016). When making future projections of TC activity, many previous studies were based on GCM simulations of future climates under various greenhouse gas emission scenarios (e.g., Camargo, 2013; Knutson & Tuleya, 2004; Wehner et al., 2015). Projected changes of TC activity in the future climate simulations were defined as model-estimated changes from the current climate simulations. Many studies concluded that the fraction of TCs becoming major storms (i.e., reaching Category 3 or higher on the Saffir-Simpson scale) will increase but overall TC frequency will decrease in a warming climate (e.g., Bindoff et al., 2013; Knutson et al., 2010; Walsh et al., 2016). However, the

estimated changes in TC activity differed considerably among the studies. For example, the projected change of TC frequency in a comprehensive assessment by Knutson et al. (2019; see their Figure 1) ranged from −28% to +22% with the median value of −14%, indicating a large uncertainty. Some recent studies projected a substantial increase in TC frequency (e.g., Bhatia et al., 2018; Emanuel, 2013; Vecchi et al., 2019).

GCM-based future TC projection studies typically use TC detection and tracking algorithms to identify explicitly simulated TC structures, such as positive temperature anomalies in the upper troposphere and closed low-level circulations of sufficient strength with local minimum in sea-level pressure (i.e., warm-cored cyclones). It has been a common practice to adjust the parameters in the TC trackers by their horizontal resolution (e.g., Camargo & Zebiak, 2002) in order to account for the fact that TCs in lower-resolution GCM simulations tend to be weaker than those in their higher-resolution counterparts.

Although high-resolution GCM simulations have been shown to perform better in simulating TC intensity than their coarse-resolution counterparts (e.g., Roberts et al., 2018; Shaevitz et al., 2014; Wehner et al., 2015), the horizontal grid spacing that is considered high-resolution for contemporary GCMs (i.e., 25 km) is still greater than the typical widths of TC eyewalls—where the strongest winds are found—which likely leads to considerably lower wind speeds. However, this does not mean that GCM-simulated TCs are fundamentally different from observed TCs. There is overwhelming evidence showing that GCM-simulated TCs qualitatively resemble and share many similarities to observed TCs, even in low-resolution models (e.g., Bengtsson et al., 1982; Chavas et al., 2017; Manganello et al., 2012; Moon et al., 2020; Murakami et al., 2015; Yamada et al., 2017). Nonetheless, as these models are not yet able to fully resolve fine-scale structures associated with high wind speeds within TC eyewalls, there are inevitably errors in the simulated TC structures. Therefore, when evaluating GCM-simulated TC intensity, one needs to take into consideration these errors in GCM-simulated TC structures.

One way of addressing the representativeness errors is to apply a horizontal resolution-dependent wind speed adjustment when comparing GCM-simulated TCs to the observations, as well as for model intercomparisons among GCMs with different horizontal resolutions. However, TC intensity in GCM simulations is typically defined as the maximum surface wind speed at a grid point near the storm center without any resolution-dependent adjustment. This definition could influence the interpretation of the performance of these simulations. Not applying a resolution-dependent wind speed adjustment when evaluating GCM-simulated TC activity in the current climate against observations could also potentially affect the reliability of future TC projections, as modeling efforts are typically directed toward improving the performance of GCM simulations against the available observations.

Walsh et al. (2007; W07) and Davis (2018; D18) have previously proposed horizontal resolution-dependent wind speed scaling adjustments that can be used when evaluating GCM simulations of TCs by constructing surface wind fields using the North Atlantic best-track data set. W07 and D18 constructed TC horizontal wind fields using different wind profile models, but both studies assumed axisymmetric TC horizontal wind fields and applied filtering to construct the resolution-dependent wind speed adjustment factors. While TCs can be approximated in the lowest order as axisymmetric vortices, TC intensity is measured by the maximum surface wind speed that is typically associated with highly asymmetric structures near the eyewall (e.g., Kepert, 2010).

The use of more realistic TC horizontal wind fields that contain asymmetries is needed to improve resolution-dependent wind speed adjustment factors, which will facilitate a more faithful evaluation of GCM-simulated TCs. In this study, we present a new method to construct a wind speed adjustment factor by analyzing two realistic high-resolution hurricane simulations and then test the new adjustment factor in several GCM simulations of TCs with different horizontal resolutions. We argue that using more realistic representations of TC surface wind fields is critical in constructing a resolution-dependent wind speed adjustment factor. Sections 2 and 3 describe the data and methodology. Results are presented in section 4, and section 5 provides a summary of the study.

2. Data

We use two hurricane simulations by Nolan et al. (2013) and Nolan and Mattocks (2014). Each simulation is a downscaling experiment of a hurricane that formed in a global simulation of the European Centre for

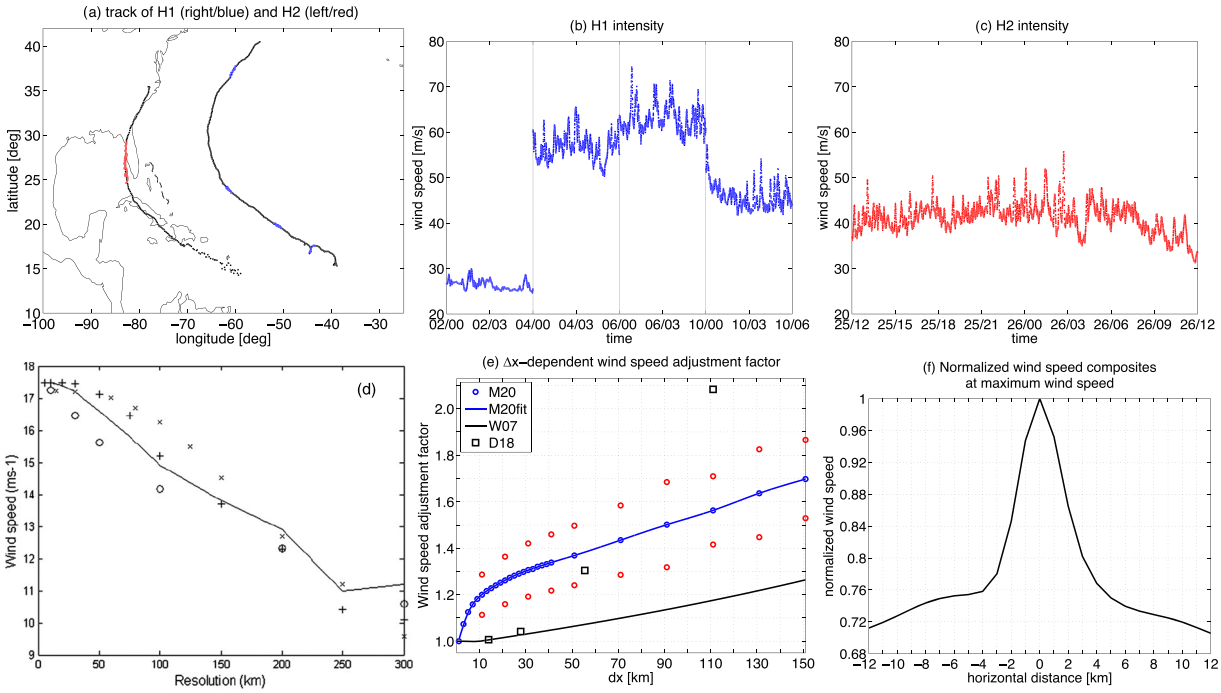

Figure 1. Panel (a) shows the H1 and H2 tracks, with blue and red dots marking the periods during which the 10-s model outputs is available. Panels (b) and (c) show the time series of the maximum surface wind speed of the H1 and H2 during which the 10-s outputs are available. Panel (d) is Figure 2 from Walsh et al. (2007) showing how the TC wind speed detecting threshold varies with horizontal resolution. Blue line in panel (e) shows the new resolution-dependent wind speed adjustment factor derived in this study, with red circles showing one standard deviation from the blue line. Black line and squares in panel (e) are calculated from the Walsh et al. (2007) and Davis (2018) results, respectively. Panel (f) shows the composite of horizontal (in the *x* and *y* directions) cross sections of normalized wind speed centered at the maximum wind speed in the H1 and H2 storms. Wind speed is normalized by the maximum wind speed in each cross section. The adjustment factors plotted as the blue line in panel (e) are 1.13, 1.20, 1.26, 1.31, 1.37, 1.56, and 1.70 at $\Delta x = 5$, 11, 21, 31, 51, 111, and 151 km, respectively.

Medium-Range Weather Forecasts (ECMWF) forecasting system with a 40-km horizontal resolution forced by the observed sea surface temperature (SST) between January 2005 and February 2006 (Masutani et al., 2009; Reale et al., 2007). This global simulation was produced without any data assimilation, so the hurricanes that formed in the free-running ECMWF simulation do not correspond to observed storms. Both hurricanes intensified from weak tropical waves in the North Atlantic when the global simulation was forced by high SST during August 2005, which was a very active North Atlantic hurricane season (Beven et al., 2008). Hereafter, the hurricane simulation of Nolan et al. (2013) is referred to as H1, while that of Nolan and Mattocks (2014) is referred to as H2. A major difference between H1 and H2 is that H2 experiences more land interactions than H1. The H1 and H2 simulations were performed with the Weather Research and Forecasting model version 3 (Skamarock et al., 2008) with 1-km horizontal grid spacing (Δx) in the vortex-following domain of 480 km by 480 km. One-kilometer horizontal resolution has been shown to realistically simulate many small-scale features of TC wind fields (e.g., Davis et al., 2008; Fierro et al., 2009; Moon & Nolan, 2015a, 2015b; Nolan, Stern, & Zhang, 2009; Nolan, Zhang, & Stern, 2009). Many aspects of the H1 and H2 simulations have been compared to observations of real hurricanes and found to be realistic by Nolan et al. (2013), Nolan and Mattocks (2014), and Nolan et al. (2014). We analyze 24 hr of 10-s surface wind fields in each hurricane simulation (i.e., a total of 48 hr, >17,000 snapshots) in order to construct a resolution-dependent wind speed adjustment factor. It is important to emphasize that 10-s model outputs can fully resolve the 1-min maximum sustained wind speed, which is the definition of TC intensity in many TC basins (e.g., Nolan et al., 2014). Figure 1a shows the center of the H1 and H2 storms, with blue and red dots marking the periods during which the 10-s model outputs are available. Figures 1b and 1c show the time series of the maximum surface wind speed of the H1 and H2 storms during which the 10-s outputs are available and saved for the analysis.

3. Methodology

We follow the methodology of Walsh et al. (2007: W07) and Davis (2018) to construct a resolution-dependent wind speed adjustment factor. W07 derived a resolution-dependent wind speed threshold for detecting TCs that is applicable to GCM simulations and reanalysis products. W07 first constructed idealized axisymmetric surface wind fields on two-dimensional cartesian grids of 1-km grid spacing using the Holland (1980) wind profile for TCs with 34-knot intensity in the 1988–2003 North Atlantic best-track data set. Then, each wind field was averaged onto coarser horizontal grids. The maximum wind speed of the coarser-resolution wind fields was defined as the TC intensity at each horizontal resolution. After processing all of the 34-kt storm wind fields, the mean of all maximum wind speeds was calculated for each horizontal resolution. These results are shown as black line in Figure 1d. No adjustment is needed for Δx smaller than 10 km for W07, while for $\Delta x = 30$ and 125 km, the adjustment factors are approximately 1.04 and 1.21, respectively. It is important to note that the W07 adjustment was intended for detecting TCs that reach 34 knots, and it is not clear if these results would be applicable for adjusting the intensity of stronger TCs.

An alternative adjustment was proposed by Davis (2018; D18; squares in Figure 1e), who constructed radial profiles of axisymmetric surface wind fields for 1988–2014 North Atlantic TCs using the wind profile model by Chavas et al. (2015) and Chavas and Lin (2016). D18 averaged the wind profiles over a radial width ($d = 8\Delta x^2/\pi r$; equation 1 of D18) determined by horizontal grid spacing (Δx) and the radial distance from the storm center (r). Therefore, more horizontal grid cells fit into an annulus of width d for greater radius values (see equation 1 and section 2.3 of D18 for additional details). For a given Δx, D18 averaged the wind profiles over all radial intervals for $r = 0$–300 nautical miles by increasing the inner edges of the averaging intervals at 1 nautical mile increments. Then, the greatest wind speed value in all averaged wind profiles is assigned as the maximum wind speed at that particular Δx. The goal of D18 was to examine how the North Atlantic TCs intensity distributions change with different Δx. Figure 1 of D18 shows how the lifetime maximum intensity of 150 kt for Hurricane Katrina (2005) would be reduced to 149, 144, 115, and 72 kt when averaged onto $\Delta x = 14$ km (≈0.125°), 28 km (≈0.25°), 56 km (≈0.5°), and 111 km (≈1°), respectively. The corresponding wind speed adjustment factors are about 1.01 at $\Delta x = 14$ km; 1.04 at $\Delta x = 28$ km; 1.30 at $\Delta x = 56$ km; and 2.08 at $\Delta x = 111$ km. These wind speed adjustment factors are similar to those of W07 for $\Delta x < 30$ km but are greater than the W07 values for $\Delta x > 50$ km.

Our proposed resolution-dependent wind speed adjustment factor is defined as the ratio of the original maximum wind speed to that diagnosed from the coarse-resolution wind field. Each hurricane surface wind field snapshot on the original 1-km grid is averaged onto coarser resolution grids, and the maximum surface wind speed of the coarser-resolution wind field is recorded as the TC intensity at that horizontal resolution. An example is shown for an individual H1 snapshot in Figures 2a to 2d where the surface wind speed on the 1-km grid is averaged onto $\Delta x = 5$-, 11-, and 31-km grids. The maximum wind speed decreases from 63.1 ms^{-1} at $\Delta x = 1$ km to 49.0 ms^{-1} at $\Delta x = 31$ km. Processing all 10-s wind field snapshots produces time series of the maximum wind speed for various horizontal resolutions. Then, these 10-s time series are averaged over time to produce time series of the 1-min averaged maximum wind speed for each horizontal resolution as in the observed TC records, and the mean of these 1-min time series is used to compute the resolution-dependent wind speed adjustment factors at various Δx values. It is assumed that the maximum wind speed at the original 1-km grid does not need adjustments.

4. Results

Blue line in Figure 1e shows the resolution-dependent wind speed adjustment factor derived from analyzing the H1 and H2 data sets. For reference, the W07 and D18 results are shown as the black line and squares. Our formulation exhibits a rapid increase in the adjustment factor for $\Delta x < 10$ km, followed by a more gradual increase for $\Delta x > 30$ km. The most noticeable differences between our adjustment factor and those from W07 and D18 are found at $\Delta x < 10$ km. While our results show a sharp increase in the adjustment factor with increasing Δx, the adjustment factors from W07 and D18 remain mostly unchanged. It is interesting to note that while our resolution-dependent wind speed adjustment factor is greater than W07 for $\Delta x > 30$ km, the slopes of both curves are quite similar.

What could be the reason for the differences between our results and those of W07 and D18 for $\Delta x < 30$ km? It may be closely related to the horizontal structures in the surface wind field associated with the wind speed

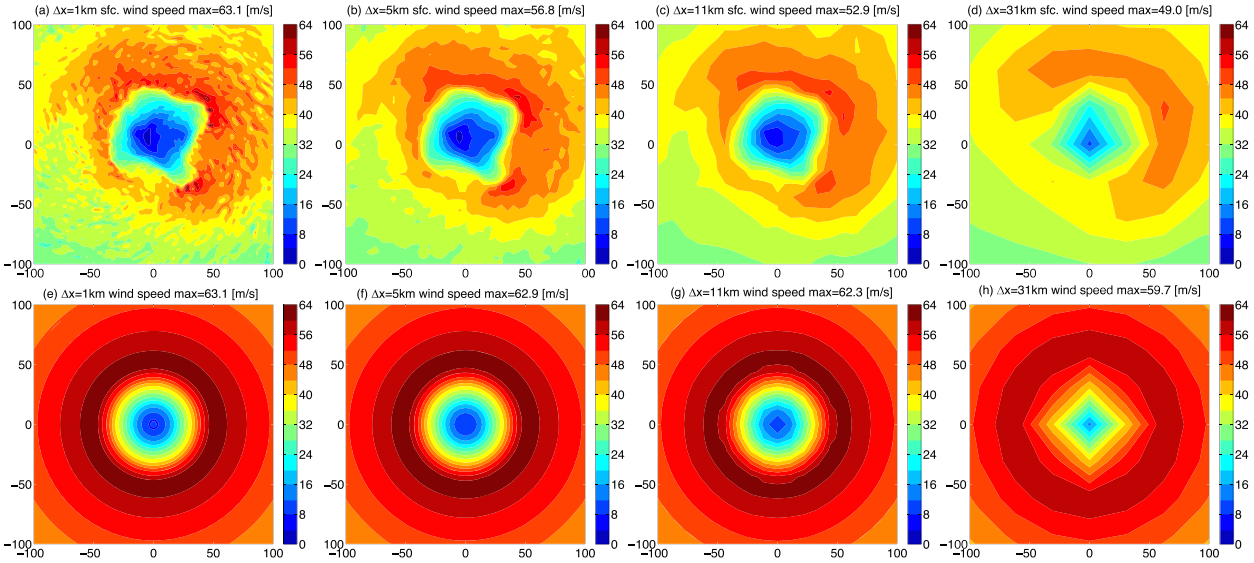

Figure 2. Panel (a) shows a surface wind speed field from the H1 storm on the 1-km horizontal grid spacing. Panels (b)–(d) show the surface wind speed field of panel (a) averaged onto 5-, 11-, and 31-km grid spacing. Panel (e) shows the azimuthally averaged surface wind speed field in panel (a), but its magnitude is increased to have the same maximum wind speed of panel (a). Panels (f)–(h) show the surface wind field of panel (e) averaged onto 5-, 11-, and 31-km grid spacing.

maxima. W07 and D18 used the axisymmetric wind fields so the maximum wind speed has an axisymmetric structure. On the other hand, the maximum wind speed in our study and in observations is typically associated with highly asymmetric, localized small patches of higher wind speeds (e.g., Kepert, 2010; Uhlhorn et al., 2014; Zhang et al., 2013), which are more susceptible to smoothing due to averaging, resulting in lower wind speed values. To illustrate this point, Figure 2e shows the azimuthally averaged wind field of Figure 2a, with the azimuthal mean profile multiplied by a constant to match the maximum wind speed of 63.1 ms^{-1} in Figure 2a. Then, Figure 2e is averaged onto the same coarse-resolution grids as in Figures 2b to 2d, and the maximum wind speed is calculated. In Figures 2e to 2h, the maximum wind speed decreases from 63.1 ms^{-1} at $\Delta x = 1$ km to 59.7 ms^{-1} at $\Delta x = 31$ km, which is a substantially smaller decrease than those noted in Figures 2a to 2d. Figures 2e to 2h translate to the wind speed adjustment factor of 1.06 at $\Delta x = 31$ km, which is in close agreement with the W07 and D18 results in Figure 1e.

Figure 1e also shows that our wind speed adjustment factor increases more slowly for $\Delta x > 10$ km than for $\Delta x < 10$ km, a feature that is absent in the W07 results. This again appears to be related to the horizontal structures surrounding the maximum wind speed. Figure 1f shows the composite horizontal cross sections of normalized H1 and H2 wind speed snapshots centered at the location of the maximum wind speed. Wind speed is normalized by the maximum wind speed in each cross section. Figure 1f indicates that there are sharp horizontal gradients in wind speed within 5 km of the maximum wind speed, but the gradients become less steep further away. This helps explain why our adjustment factor in Figure 1e increases more slowly for $\Delta x > 10$ km. As Δx increases beyond 10 km, averages are performed over regions in which the wind speed does not decrease as quickly as in the 5-km neighborhoods, resulting in a smaller decrease of the maximum wind speed with increasing Δx. This in turn leads to a smaller increase of the corresponding wind speed adjustment factor.

How different would GCM-simulated TC intensity distributions be if our new resolution-dependent wind speed adjustment is used? Figure 3 shows the TC intensity distributions from three GCM [(a) 0.25° NCAR CAM5 (1996–1997); (b) 0.5° GFDL HiRAM (1984–1985); and (c) 1° GFDL AM4 developmental version (2008–2012)] simulations of North Atlantic and eastern and western North Pacific TCs. TCs in these simulations have been examined by Kim et al. (2018), Wing et al. (2019), Moon et al. (2020), and Camargo et al. (2020), and more details of the simulations can be found therein. For reference, the observed TC intensity distributions for the same regions and periods are shown as black lines, which use the National Hurricane Center best-track data for the North Atlantic and eastern North Pacific TCs and the Joint Typhoon Warning Center best-track data for the western North Pacific TCs. TC intensity distributions

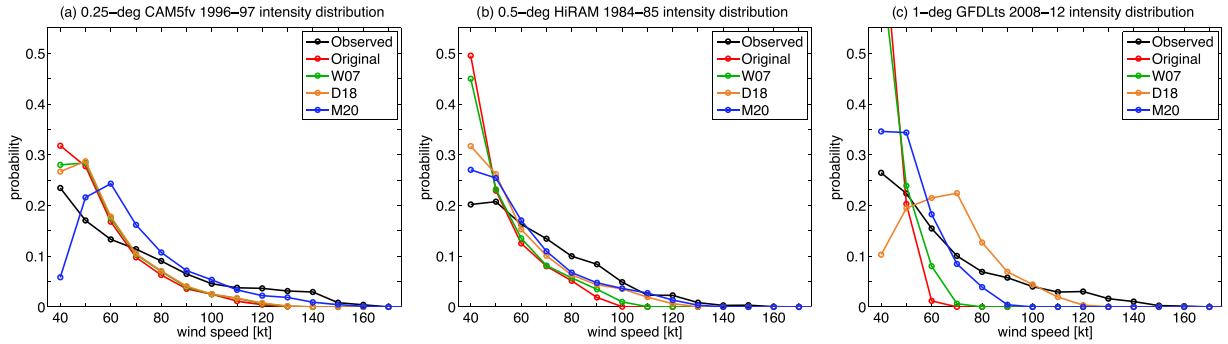

Figure 3. TC intensity distributions in (a) 0.25° CAM5, (b) 0.5° HiRAM, and (c) 1° AM4d global climate model simulations in the North Atlantic and North Pacific TC basins during (a) 1996–1997, (b) 1984–1985, and (c) 2008–2012, respectively. The original simulated TC intensity is plotted in red, while green, orange, and blue lines show the TC intensity distributions that are adjusted with the results of Walsh et al. (2007; W07), Davis (2018; D18), and present study (M20). Black lines show the observed intensity distributions for the same period and regions.

obtained from tracking the model TCs without any resolution-dependent adjustments are plotted in red lines, while green, orange, and blue lines show the intensity distributions when they are adjusted with the values of W07, D18, and using our new proposed adjustment (M20). Red lines in Figure 3 indicate that GCM simulations are not able to reproduce the high wind speed tails (>95 knots, i.e., Category 3 storms) of the observed intensity distributions, especially for the low-resolution simulations.

Applying the W07 adjustment (green) moves the intensity curves closer to the observed distributions, but there is still a substantial low-intensity bias. The D18 adjustment (orange) curve is very similar to the W07 curve for the 0.25° simulation (Figure 3a). In contrast, the D18-adjusted intensity distributions for the 0.5° (Figure 3b) and 1° (Figure 3c) simulations are much closer to the observed distributions than either the original or W07-adjusted distributions. Furthermore, there is a greater frequency of TCs in the high wind speed tails in the D18 curves in Figures 3b and 3c. When the TC intensity is corrected using our new adjustment factor (blue), the TC intensity distributions are closer to the observed distributions than the other two adjustments for the 0.25° and 0.5° simulations (Figures 3a and 3b). While the occurrence of strong TCs increases, a slight low-intensity bias remains at the high wind speed tail. While all adjusted TC intensity distributions for the 1° simulation lead to a higher frequency of stronger TCs, the D18 adjustment produces the intensity distribution closest to the observed curve. Figure 3b shows that the D18 and our adjusted distributions are very similar, with similar values of the adjustment factors for $\Delta x = 0.5°$ (see Figure 1e).

It is evident from Figure 3 that depending on whether TC intensity is adjusted or not and which adjustment formulation is used, the model TC intensity distributions can be characterized in substantially different ways, which could also result in different projections for future TC intensity changes from the same GCM simulations. However, as discussed earlier, typically no resolution-dependent adjustments have been applied in previous studies, which raises the possibility that widely discussed interpretation of low-intensity bias in GCM-simulated TCs might be smaller than previously thought.

5. Summary

This study presents a new method to construct a horizontal resolution-dependent wind speed adjustment factor that can be used for evaluating intensity of TCs in GCM simulations. The new wind speed adjustment factor shows a faster increase with increasing horizontal grid spacing than previous studies for $\Delta x < 30$ km. This difference is likely due to the use of more realistic surface wind fields than those used in the previous studies. The wind fields analyzed in this study contain numerous highly asymmetric, localized wind structures that are absent in smoothly varying axisymmetric wind fields.

This study is based on the analysis of 48 hr of 10-s surface wind fields of two TC simulations only. Therefore, it would be helpful to include additional simulations in a follow-up study to construct a more comprehensive wind speed adjustment factor that could potentially incorporate other relevant parameters, such as storm structures, size or motion, or environmental vertical wind shear. The differences between our formulation and those of W07 and D18 for $\Delta x < 30$ km can be attributed to the horizontal structures surrounding the

maximum wind speed in the analyzed wind fields. Given the large sample size used (>17,000 snapshots), the rapid increase in the wind speed adjustment factor with increasing Δx in our formulation is likely to be a very robust feature.

It is clear that a resolution-dependent wind speed adjustment factor is needed when examining GCM TC simulations against the observations and among models of different horizontal resolution (Figure 3). Applying our new resolution-dependent adjustment factor to several GCM simulations indicates that the common interpretation of low-intensity bias in GCM-simulated TCs may be slightly overstated. Not using a resolution-dependent adjustment could influence the interpretation of how well GCMs simulate the observed TC activity, and this can affect the directions of future model development efforts. In addition, projected future changes of TC activity, which are often estimated as the differences from the present-day simulations, can be affected by whether a resolution-dependent adjustment is applied or not.

We are currently evaluating TC activity in additional GCM simulations with different horizontal resolutions using the newly constructed resolution-dependent adjustment factor. Sensitivity of TC intensity in current and future climate simulations to horizontal resolution-dependent wind speed adjustment will be examined in detail in the future. It is important to mention that there are other methods to construct a resolution-dependent adjustment factor, which typically use long-term GCM simulations to formulate statistical resolution-dependent adjustment factors (e.g., Sugi et al., 2017; Zhao & Held, 2010). It will be of interest to evaluate how the adjustment factor of this study compares to those that are constructed differently. In addition, Chavas et al. (2017) and Murata et al. (2020) have recently suggested that minimum central sea-level pressure could be used as an alternative metric for TC intensity in GCM simulations. Constructing a resolution-dependent adjustment factor for central sea-level pressure could be considered as a future study.

Data Availability Statement

The data underlying the figures from this work are available at https://osf.io/n4uj9/.

Acknowledgments

We are grateful to David S. Nolan for generously sharing the WRF TC simulations. This study is supported by the National Oceanic and Atmospheric Administration (NOAA) Climate Program Office (CPO) Modeling, Analysis, Predictions and Projections (MAPP) Program Grants NA15OAR4310087, NA15OAR4310095, NA18OAR4310270, NA18OAR4310276, and NA18OAR4310277 and by the Department of Energy (DOE) Regional and Global Model Analysis (RGMA) Program Grant DE-SC0016223. DK was also supported by KMA R&D Program Grant KMI2018-03110. KAR was partially supported by DOE RGMA program grant DE-SC0016605. MFW was funded by the Regional and Global Model Analysis program in the Office of Biological and Environmental Research, US Department of Energy and used resources at the National Energy Research Supercomputer Center. We thank Jun A. Zhang and an anonymous reviewer for constructive reviews.

References

Bengtsson, L., Böttger, H., & Kanamitsu, M. (1982). Simulation of hurricane-type vortices in a general circulation model. *Tellus*, *34*(5), 440–457. https://doi.org/10.3402/tellusa.v34i5.10830

Beven, J. L., Avila, L. A., Blake, E. S., Brown, D. P., Franklin, J. L., Knabb, R. D., et al., (2008). Atlantic hurricane season of 2005. *Monthly Weather Review*, *136*(3), 1109–1173. https://doi.org/10.1175/2007MWR2074.1

Bhatia, K., Vecchi, G., Murakami, H., Underwood, S., & Kossin, J. (2018). Projected response of tropical cyclone intensity and intensification in a global climate model. *Journal of Climate*, *31*(20), 8281–8303. https://doi.org/10.1175/JCLI-D-17-0898.1

Bindoff, N. L., et al. (2013). Detection and attribution of climate change: From global to regional. Climate Change 2013: The Physical Science Basis. In T. F. Stocker et al. (Eds.), T. F. Stockeret al., Eds., Cambridge University press, 867–952

Camargo, S. J. (2013). Global and Regional Aspects of Tropical Cyclone Activity in the CMIP5 Models. *Journal of Climate*, *26*, 9880–9902. https://doi.org/10.1175/JCLI-D-12-00549.1

Camargo, S. J., Giulivi, C. F., Sobel, A. H., Wing, A. A., Kim, D., Moon, Y., et al. (2020). Characteristics of model tropical cyclone climatology and the large-scale environment. *Journal of Climate*, *33*(11), 4463–4487. https://doi.org/10.1175/JCLI-D-19-0500.1

Camargo, S. J., & Wing, A. A. (2016). Tropical cyclones in climate models. *WIREs Climate Change*, *7*(2), 211–237. https://doi.org/10.1002/wcc.373

Camargo, S. J., & Zebiak, S. E. (2002). Improving the detection and tracking of tropical cyclones in atmospheric general circulation models. *Weather and forecasting*, *17*(6), 1152–1162. https://doi.org/10.1175/1520-0434(2002)017%3;1152:ITDATO%3E;2.0.CO;2

Chavas, D. R., & Lin, N. (2016). A model for the complete radial structure of the tropical cyclone wind field. Part II: Wind field variability. *Journal of the Atmospheric Sciences*, *73*(8), 3093–3113. https://doi.org/10.1175/JAS-D-15-0185.1

Chavas, D. R., Lin, N., & Emanuel, K. (2015). A model for the complete radial structure of the tropical cyclone wind field. Part I: Comparison with observed structure. *Journal of the Atmospheric Sciences*, *72*(9), 3647–3662. https://doi.org/10.1175/JAS-D-15-0014.1

Chavas, D. R., Reed, K. A., & Knaff, J. A. (2017). Physical understanding of the tropical cyclone wind-pressure relationship. *Nature Communications*, *8*(1), 1360. https://doi.org/10.1038/s41467-017-01546-9

Davis, C., Wang, W., Chen, S. S., Chen, Y., Corbosiero, K., DeMaria, M., et al. (2008). Prediction of landfalling hurricanes with the advanced hurricane WRF model. *Monthly Weather Review*, *136*(6), 1990–2005. https://doi.org/10.1175/2007MWR2085.1

Davis, C. A. (2018). Resolving tropical cyclone intensity in models. *Geophysical Research Letters*, *45*, 2082–2087. https://doi.org/10.1002/2017GL076966

Emanuel, K. A. (2013). Downscaling CMIP5 climate models shows increased tropical cyclone activity over the 21st century. *Proceedings of the National Academy of Sciences*, *110*, 12219–12224. https://doi.org/10.1073/pnas.1301293110

Fierro, A. O., Rogers, R. F., Marks, F. D., & Nolan, D. S. (2009). The impact of horizontal grid spacing on the microphysical and kinematic structures of strong tropical cyclones simulated with the WRF-ARW model. *Mon. Wea. Rev.*, *137*(11), 3717–3743. https://doi.org/10.1175/2009MWR2946.1

Holland, G. J. (1980). An analytic model of the wind and pressure profiles in hurricanes. *Mon. Wea. Rev.*, *108*(8), 1212–1218. https://doi.org/10.1175/1520-0493(1980)108%3;1212:AAMOTW%3E;2.0.CO;2

Kepert, J. D. (2010). Tropical cyclone structure and dynamics. *Global Perspectives on Tropical Cyclones.*, 3–53. https://doi.org/10.1142/9789814293488_0001

Kim, D., Moon, Y., Camargo, S. J., Wing, A. A., Sobel, A. H., Murakami, H., et al. (2018). Process-oriented diagnosis of tropical cyclones in high-resolution GCMs. *Journal of Climate*, *31*(5), 1685–1702. https://doi.org/10.1175/JCLI-D-17-0269.1

Knutson, T., Camargo, S. J., Chan, J. C., Emanuel, K., Ho, C., Kossin, J., et al. (2019). Tropical cyclones and climate change assessment: Part II. Projected response to anthropogenic warming. *Bulletin of the American Meteorological Society*, *101*(3), E303–E322. https://doi.org/10.1175/BAMS-D-18-0194.1

Knutson, T. R., McBride, J. L., Chan, J., Emanuel, K., Holland, G., Landsea, C., et al. (2010). Tropical cyclones and climate change. *Nature Geoscience*, *3*(3), 157–163. https://doi.org/10.1038/ngeo779

Knutson, T. R., & Tuleya, R. E. (2004). Impact of CO2-Induced Warming on Simulated Hurricane Intensity and Precipitation: Sensitivity to the Choice of Climate Model and Convective Parameterization. *Journal of Climate*, *17*, 3477–3495. https://doi.org/10.1175/1520-0442(2004)017<3477:IOCWOS>2.0.CO;2

Manganello, J. V., Hodges, K. I., Kinter, J. L. III, Cash, B. A., Marx, L., Jung, T., et al. (2012). Tropical cyclone climatology in a 10-km global atmospheric GCM: Toward weather-resolving climate modeling. *Journal of Climate*, *25*(11), 3867–3893. https://doi.org/10.1175/JCLI-D-11-00346.1

Masutani, M., Andersson, E., Riishojgaard, L. P., Weng, F., Errico, R. M., Woollen, J., et al. (2019). International collaborative Joint OSSEs -- Toward reliable and timely assessment of future observing systems. *Preprints in Anthony Hollingsworth Symposium Posters*. Retrieved from https://ams.confex.com/ams/89annual/techprogram/paper_149641.htm, https://ams.confex.com/ams/pdfpapers/149641.pdf

Moon, Y., Kim, D., Camargo, S. J., Wing, A. A., Sobel, A. H., Murakami, H., et al. (2020). Azimuthally averaged wind and thermodynamic structures of tropical cyclones in global climate models and their sensitivity to horizontal resolution. *Journal of Climate*, *33*(4), 1575–1595. https://doi.org/10.1175/JCLI-D-19-0172.1

Moon, Y., & Nolan, D. S. (2015a). Spiral rainbands in a numerical simulation of Hurricane Bill (2009a). Part I: Structures and comparisons to observations. *Journal of the Atmospheric Sciences*, *72*(1), 164–190. https://doi.org/10.1175/JAS-D-14-0058.1

Moon, Y., & Nolan, D. S. (2015b). Spiral rainbands in a numerical simulation of Hurricane Bill (2009b). Part II: Propagation of inner rainbands. *Journal of the Atmospheric Sciences*, *72*(1), 191–215. https://doi.org/10.1175/JAS-D-14-0056.1

Murakami, H., Vecchi, G. A., Underwood, S., Delworth, T. L., Wittenberg, A. T., Anderson, W. G., et al. (2015). Simulation and prediction of Category 4 and 5 hurricanes in the high-resolution GFDL HiFLOR coupled climate model. *Journal of Climate*, *28*(23), 9058–9079. https://doi.org/10.1175/JCLI-D-15-0216.1

Murata, A., Watanabe, S-I., Sasaki, H., Kawase, H. & Nosaka, M. (2020). The development of a resolution-independent tropical cyclone detection scheme for high-resolution climate model simulations. *Journal of the Meteorological Society of Japan*, https://doi.org/10.2151/jmsj.2019-035, *97*, 2, 519, 531

Nolan, D. S., Atlas, R., Bhatia, K. T., & Bucci, L. R. (2013). Development and validation of a hurricane nature run using the joint OSSE nature run and the WRF model. *Journal of Advances in Modeling Earth Systems*, *5*, 382–405. https://doi.org/10.1002/jame.20031

Nolan, D. S., & Mattocks, C. A. (2014). Development and evaluation of the second hurricane nature run using the joint OSSE nature run and the WRF model. Preprint, 31st Conference on Hurricanes and Tropical Meteorology, San Diego, CA.

Nolan, D. S., Stern, D. P., & Zhang, J. A. (2009). Evaluation of planetary boundary layer parameterizations in tropical cyclones by comparison of in situ observations and high-resolution simulations of Hurricane Isabel (2003). Part II: Inner-core boundary layer and eyewall structure. *Monthly Weather Review*, *137*(11), 3675–3698. https://doi.org/10.1175/2009MWR2786.1

Nolan, D. S., Zhang, J. A., & Stern, D. P. (2009). Evaluation of planetary boundary layer parameterizations in tropical cyclones by comparison of in situ observations and high-resolution simulations of Hurricane Isabel (2003). Part I: Initialization, maximum winds, and the outer-core boundary layer. *Monthly Weather Review*, *137*(11), 3651–3674. https://doi.org/10.1175/2009MWR2785.1

Nolan, D. S., Zhang, J. A., & Uhlhorn, E. W. (2014). On the limits of estimating the maximum wind speeds in hurricanes. *Mon. Wea. Rev.*, *142*(8), 2814–2837. https://doi.org/10.1175/MWR-D-13-00337.1

Reale, O., Terry, J., Masutani, M., Andersson, E., Riishojgaard, L. P., & Jusem, J. C. (2007). Preliminary evaluation of the European Centre for Medium-Range Weather Forecasts' (ECMWF) nature run over the tropical Atlantic and African monsoon region. *Geophysical Research Letters*, *34*, L22810. https://doi.org/10.1029/2007GL031640

Roberts, M. J., Vidale, P. L., Senior, C., Hewitt, H. T., Bates, C., Berthou, S., et al. (2018). The benefits of global high resolution for climate simulation: Process understanding and the enabling of stakeholder decisions at the regional scale. *Bull. Amer. Meteor. Soc.*, *99*(11), 2341–2359. https://doi.org/10.1175/BAMS-D-15-00320.1

Shaevitz, D. A., Camargo, S. J., Sobel, A. H., Jonas, J. A., Kim, D., Kumar, A., et al. (2014). Characteristics of tropical cyclones in high-resolution models in the present climate. *Journal of Advances in Modeling Earth Systems*, *6*, 1154–1172. https://doi.org/10.1002/2014MS000372

Skamarock, W. C., Klemp, J. B., Dudhia, J., Gill, D. O., Barker, D. M., Duda, M. G., et al. (2008). *A description of the advanced research WRF version 3, NCAR Tech. Note, 475+STR* (p. 113). Boulder, CO: University Corporation for Atmospheric Research. https://doi.org/10.5065/D68S4MVH

Sugi, M., Murakami, H., & Yoshida, K. (2017). Projection of future changes in the frequency of intense cyclones. *Climate Dynamics*, *49*(1-2), 619–632. https://doi.org/10.1007/s00382-016-3361-7

Uhlhorn, E. W., Klotz, B. W., Vukicevic, T., Reasor, P. D., & Rogers, R. F. (2014). Observed hurricane wind speed asymmetries and relationships to motion and environmental shear. *Mon. Wea. Rev.*, *142*(3), 1290–1311. https://doi.org/10.1175/MWR-D-13-00249.1

Vecchi, G. A., Delworth, T. L., Murakami, H., Underwood, S. D., Wittenberg, A. T., Zeng, F., et al. (2019). Tropical cyclone sensitivities to CO2 doubling: Role of atmospheric resolution, synoptic variability and background climate changes. *Climate Dynamics*, *53*(9-10), 5999–6033. https://doi.org/10.1007/s00382-019-04913-y

Walsh, K. J., Fiorino, M., Landsea, C. W., & McInnes, K. L. (2007). Objectively determined resolution-dependent threshold criteria for the detection of tropical cyclones in climate models and reanalyses. *Journal of Climate*, *20*(10), 2307–2314. https://doi.org/10.1175/JCLI4074.1

Walsh, K. J., McBride, J. L., Klotzbach, P. J., Balachandran, S., Camargo, S. J., Holland, G., et al. (2016). Tropical cyclones and climate change. *WIREs Climate Change*, *7*(1), 65–89. https://doi.org/10.1002/wcc.371

Wehner, M., Prabhat, K. A., Reed, D., Stone, W. D. C., & Bacmeister, J. (2015). Resolution dependence of future tropical cyclone projections of CAM5.1 in the U.S. CLIVAR Hurricane Working Group idealized configurations. J. *Climate*, *28*(10), 3905–3925. https://doi.org/10.1175/JCLI-D-14-00311.1

Wing, A. A., Camargo, S. J., Sobel, A. H., Kim, D., Moon, Y., Murakami, H., et al. (2019). Moist static energy budget analysis of tropical cyclone intensification in high-resolution climate models. *Journal of Climate*, *32*(18), 6071–6095. https://doi.org/10.1175/JCLI-D-18-0599.1

Yamada, Y., Satoh, M., Sugi, M., Kodama, C., Noda, A. T., Nakano, M., & Nasuno, T. (2017). Response of tropical cyclone activity and structure to global warming in a high-resolution global nonhydrostatic model. *Journal of Climate*, *30*(23), 9703–9724. https://doi.org/10.1175/JCLI-D-17-0068.1

Zhang, J. A., Rogers, R. F., Reasor, P. D., Uhlhorn, E. W., & Marks, F. D. (2013). Asymmetric hurricane boundary layer structure from dropsonde composites in relation to the environmental vertical wind shear. *Monthly Weather Review*, *141*(11), 3968–3984. https://doi.org/10.1175/MWR-D-12-00335.1

Zhao, M., & Held, I. M. (2010). An analysis of the effect of global warming on the intensity of Atlantic hurricanes using a GCM with statistical refinement. *Journal of Climate*, *23*(23), 6382–6393. https://doi.org/10.1175/2010JCLI3837.1